https://doi.org/10.1016/j.tws.2020.107215

Structural behaviour and design of high strength steel CHS T-joints

Xiaoyi Lan[a,1,*], Tak-Ming Chan[b], Ben Young[b]

[a] School of Civil and Environmental Engineering, Nanyang Technological University, Singapore

[b] Dept. of Civil and Environmental Engineering, The Hong Kong Polytechnic University, Hong Kong, China

[1] Formerly, Dept. of Civil and Environmental Engineering, The Hong Kong Polytechnic University, Hong Kong, China

*xiaoyi.lan@connect.polyu.hk

Abstract: This paper investigates the structural behaviour of high strength steel (HSS) circular hollow section (CHS) T-joints under brace axial compression. Finite element analysis on CHS T-joints using S460, S700, S900 and S1100 steel was conducted, and the chord plastification failure was examined. The effect of heat affected zones (HAZ) on the joint behaviour and influences of the steel grade, brace to chord diameter ratio (β) and chord diameter to wall thickness ratio (2γ) on the suitability of the CIDECT mean strength equations for HSS CHS T-joints were evaluated. The effect of HAZ on the initial stiffness of HSS CHS T-joints is found to be insignificant. The material softening in HAZ can lower the joint strength; however, the joint strength reduction is less pronounced. In general, the influence of β ratio on the suitability of the CIDECT mean strength equations for HSS CHS T-joints is minor. The CIDECT mean strength prediction is relatively accurate for S460 CHS T-joints and becomes increasingly unconservative for higher steel grade and larger 2γ ratio. This is because the improved yield stresses of HSS generally could not be fully utilised due to the adopted CIDECT indentation limit of 3% of chord diameter. It is suggested to tighten the range of 2γ ratio to be $2\gamma \leq 40$ for steel grades ranging from S460 to S700 and $2\gamma \leq 30$ for steel grades greater than S700 up to S1100 to allow for more effective use of HSS. The CIDECT validity range of $0.2 \leq \beta \leq 1.0$ is also recommended for steel grades ranging from S460 to S1100. Mean and design strength equations modified from the CIDECT strength equations were proposed for HSS CHS T-joints with 2γ and β

ratios which are within the suggested ranges.

Keywords: Chord plastification; Circular hollow section; High strength steel; Structural design; T-joint

1. Introduction

High strength steel (HSS) with nominal yield stresses higher than 450 MPa features with advantageous strength-to-weight ratios and is increasingly popular in onshore and offshore tubular structures [1]. The merits of HSS tubular structures are in the reduction of member sizes and subsequent costs of fabrication, transportation and construction. The lower consumption of steel materials can also contribute to the resource-saving, carbon footprint reduction and thus the sustainable development of the infrastructure sector. Design rules for HSS tubular members have been proposed (e.g. Lan et al. [2, 3] and Ma et al. [4]); however, research and design guidance for HSS tubular joints which are also indispensable components in HSS tubular structures remain limited.

Current design guides and codes are originally developed for normal strength steel tubular joints. The extension of the codified strength equations to the design of tubular joints using steel grades greater than S355 comes with additional reduction factors of joint strength. The CIDECT design guides [5, 6] impose a reduction factor of 0.9 and the limitation on the yield stress to 0.8 times the ultimate stress. Likewise, the current Eurocode 3 [7, 8] stipulates reduction factors of 0.9 for steel grades beyond S355 up to S460 and 0.8 for steel grades greater than S460 up to S700. However, the suitability of such design rules remains controversial and has been re-evaluated in some recent investigations on HSS joints. A review on the research advances of HSS rectangular hollow section (RHS) joints is elaborated by Lan and Chan [9] and the recent studies on HSS circular hollow section (CHS) joints are summarised herein. The test and numerical investigations conducted by Puthli et al. [10] and Lee et al. [11] show that the Eurocode design strengths without using the reduction factors are higher than the test and numerical static strengths of CHS X-joints using steel grades from S460 to S770. Lan et al. [12-14] experimentally and numerically assessed the structural performance of CHS X-joints using steel grades from S460 to S1100 which failed by chord plastification. It is found that the deformation capacity of test specimens could be considered as reasonably sufficient, and the effect of material softening in the heat affected zones (HAZ) on the joint strength is less significant than the pronounced material softening. The CIDECT mean strength prediction is increasingly unconservative for higher steel grades, and design rules were proposed for the X-joints. Lan et al. [14] also examined the chord plastification in CHS T-joint specimens with a nominal yield stress of 960 MPa. It is found that the deformation capacity of test specimens was reasonably sufficient, and the CIDECT and Eurocode mean strength predictions are unconservative. However, comprehensive research on HSS CHS T-joints remains limited.

An extensive finite element (FE) study is presented herein on the chord plastification in CHS T-joints under brace axial compression and using steel grades of S460, S700, S900 and S1100. FE analysis was conducted to examine the effect of HAZ and structural performance of HSS CHS T-joints. The CIDECT mean strength equations were assessed. Design rules which allow for reasonably effective use of HSS were proposed for HSS CHS T-joints in steel grades ranging from S460 to S1100.

2. Finite element analysis

2.1. Finite element model

Fig. 1 shows the configuration and notations of CHS T-joints. Lan et al. [14] conducted an experimental investigation on seven CHS T-joints which failed by chord plastification as illustrated in Fig. 2. Table 1 shows the measured joint parameters of the test specimens with a nominal yield stress of the chord (f_y) of 960 MPa. The angle between the brace and chord (θ) for the T-joints was 90°. The ratio (β=d_1/d) of brace to chord diameter ranged from 0.60 to 0.93 and the ratio (2γ=d/t) of chord diameter to wall thickness varied from 42.8 to 54.2. A robotic welding machine was used to perform the gas metal arc welding (GMAW) with a low heat input of 0.38 kJ/mm, and the measured material properties of heat affected zones (HAZ) were comparable with those of the base metal. Axial compression was applied at the brace end and the chord ends sat on rollers through the chord end seatings. The distance (L_s) between the centres of two rollers was set to be six times of the nominal chord diameter as shown in Table 1. The chord face indentation at the chord crown and maximum chord side wall deflection were obtained by using calibrated linear variable displacement transducers (LVDTs). It should be noted that the chord face indentation in this study was taken as the difference of displacements at the chord crown and the position at mid-span of the chord bottom i.e. the chord face indentation was obtained by subtracting the global bending deflection at the mid-span of the chord from the obtained deformation at the chord crown. The chord end failure occurred in the T1 specimen at large deformation exceeding the CIDECT indentation limit of 3%*d* [6], and thus the chord ends of the other six specimens were horizontally clamped by G-clamps and were vertically stiffened using the internal supports to avoid the chord end failure. Figs. 3-4 show the obtained load-deformation curves and Table 1 summarises the static strengths (N_{Test}) of test specimens. The static strength of CHS T-joints herein is taken as the peak load or the load at the indentation limit of 3%*d*, whichever occurs earlier, in line with the CIDECT design guide [6].

FE analysis on HSS CHS T-joints was performed using ABAQUS [15]. A FE model was developed and validated against the test results reported by Lan et al. [14]. The measured dimensions of test specimens as shown in Table 1 were adopted. A four-node shell element with reduced integration (S4R) was used to model the brace and chord members without weld modelling. A suitable mesh size of 8 mm determined by a mesh sensitivity study was employed. The true stress and logarithmic plastic strain which were converted from the measured engineering stress and strain in the coupon tests [14] were used. The material softening in the HAZ of the chord was not modelled because it was found to be insignificant [14]. The Poisson's ratio (v) of steel in this study was taken as 0.3. The von-Mises yield criterion and isotropic strain hardening rules were adopted. Fig. 5 shows the boundary conditions employed which were chosen to closely simulate the test set-up [14]. The degrees of freedom of all nodes at the brace end were coupled to a concentric reference point (RP-1) by using rigid body constraints. All degrees of freedom of the brace reference point were restricted except the brace axial translation. The degrees of freedom of all nodes of the contact surface (i.e. the yellow surfaces in Fig. 5) of each chord end to the chord end seating with a central angle of 120° were coupled to a reference point (RP-2 and RP-3), and only the chord axial translation and chord in-plane rotation of the reference point were allowed. For the test specimens except the T1 specimen, the chord ends were stiffened to avoid the chord end failure. In order to simulate the stiffening effect, the contact region of each chord end to each stiffener was simplified as a contact line (i.e. the green lines in Fig. 5) whose degrees of freedom of all nodes were coupled to a reference point (RP-4 to RP-9), and the displacement along the stiffening direction of the reference point was restricted. The distance of all reference points for the chord (RP-2 to RP-9) was 45 mm away from the chord end where the rollers were placed, and the length of the contact surfaces and lines along the chord axial direction was 120 mm.

Fig. 2 shows that the predicted failure mode of chord plastification can closely mirror the test observation. Figs. 3-4 demonstrate that the FE model produces accurate prediction of the load-deformation curves when compared with the test curves. Table 1 summarises the static strengths of the CHS T-joint specimens obtained from the FE simulations (N_{FE}) and tests (N_{Test}). The mean value of $N_{\mathrm{Test}}/N_{\mathrm{FE}}$ ratio is 1.02 with corresponding coefficient of variation (COV) of 0.053, and thus the FE joint strengths agree well with the test strengths. It is therefore concluded that the developed FE model without weld modelling can produce accurate prediction of the structural behaviour of CHS T-joints and is suitable for the subsequent FE simulations.

2.2. Effects of heat affected zones

The heat input of welding can alter the material properties of heat affected zones (HAZ), which mainly depend on the steel material, heat input, welding type and cooling time [13]. Stroetmann et al. [16] found that the material softening occurred in the HAZ of thermo-mechanical controlled processing (TMCP) S700 steel and was not observed in the HAZ of quenching and tempering (QT)

S690Q and S960Q steel and TMCP S500M steel. Siltanen et al. [17] also reported that the material softening for directing quenching (DQ) S960 steel was around 20% while that of QT S960 steel was insignificant. The results demonstrate that the material softening in the HAZ can be more significant for higher steel grades and more pronounced for TMCP and DQ HSS than that of the traditional QT HSS. Higher heat input can result in larger material strength reduction in the HAZ of HSS [18]. Comprehensive welding guidance is urgently needed for HSS in order to mitigate the possible adverse effects of the HAZ in HSS structures.

It is significant to examine the effects of material softening in the HAZ on the structural behaviour of HSS CHS T-joints because the material strength reduction can occur in HSS tubular structures. FE analysis was conducted on CHS T-joints in S900 and S1100 steel because the material softening is less pronounced for lower steel grades [16, 18]. The measured dimensions of the T4 specimen listed in Table 1 were employed for the FE simulations. The geometric parameters of the four FE specimens (T4-1, T4-2, T4-3 and T4-4) are summarised in Table 2 and other parameters not listed are the same as those of the T4 specimen. The parameter ranges of these specimens are $0.3 \le \beta \le 0.8$ and $18.0 \le 2\gamma \le 52.8$. The developed FE model with chord end stiffening described in Section 2.1 of this paper was adopted.

Fig. 6 illustrates the HAZ in the chord of analysed CHS T-joints using S900 and S1100 steel, and the sizes and material strength reduction of the HAZ were determined in line with Lan et al. [13]. The width and depth of the HAZ at the brace-chord intersection were taken as t_1+w+12 mm and t, respectively. The physical appearance of the fillet weld was not modelled in the FE simulations because the validation study described in Section 2.1 of this paper shows that the developed FE model without weld modelling can produce accurate prediction of the structural behaviour of CHS T-joints. However, the weld leg size of the fillet weld (w) as shown in Fig. 6 was considered in the modelling of HAZ. The HAZ in the brace was not modelled as the brace cross-section capacity was higher than the joint strength. The reduction of yield stress (f_y) and ultimate stress (f_u) of the HAZ near the weld which is in red colour (see Fig. 6) was taken as 20% and 30% for S900 and S1100 steel, respectively, and that of the HAZ far from the weld (in blue colour) equals to 10% and 15% for S900 and S1100 steel, respectively. The ultimate strain at ultimate stress (ε_u) of the HAZ in S900 and S1100 steel near the weld (in red) was taken as 2.1 and 3.5 times the values of ε_u of base metals, respectively [18]. The elastic modulus (E) of base metals was adopted for the HAZ. Table 3 summarises the material parameters adopted for the CHS T-joints. The number following the letter R denotes the percentage of material strength reduction when compared with the base metals. Fig. 7 shows the adopted engineering stress-strain curves obtained from the reported stress-strain curve model [19]. It is noted that the proportional elongations at fracture of ultra-high strength steel measured in tests varying from 13% to 15% for S900 steel and ranging from 12% to 13% for S1100 steel [19] were relatively small when compared with normal strength steel.

Figs. 8-9 show the obtained load-indentation curves of S900 and S1100 CHS T-joints without and with HAZ. The effect of the material softening in HAZ on the initial stiffness of the joints is found to be minor. This is because the initial stiffness is mainly governed by the steel elastic modulus and the joint geometric parameters. This therefore indicates that the effect of HAZ can be neglected when the elastic analysis on HSS tubular structures is performed. However, the HAZ can lower the stiffness and static strength of HSS CHS T-joints when inelastic deformations occur. The static strengths of the T-joints without HAZ (N_{u1}) and with HAZ (N_{u2}) are tabulated in Table 2. The joint strength reduction ranges from 2% to 7% for S900 CHS T-joints and varies from 4% to 10% for S1100 CHS T-joints. The joint strength reduction resulted from the HAZ is less significant when compared with the pronounced material softening in the HAZ. This could be attributed to the redistribution of plastic stresses in HAZ to nearby base metals and the under-utilisation of the improved yield stresses of HSS in the CHS T-joints which will be discussed in Section 3.2 of this paper. It is also noteworthy that the material strength reduction and sizes of HAZ adopted in the FE simulations for the CHS T-joints are relatively large and could be smaller if optimised welding parameters are employed which could lead to minor joint strength reduction. Furthermore, the joint strength reduction could be less significant for the CHS T-joints using QT HSS than that of the T-joints in TMCP or DQ HSS because of less pronounced material strength reduction in HAZ of QT HSS [16-18]. The HAZ is therefore not explicitly modelled in the subsequent parametric study. However, conservative strength equations were proposed for HSS CHS T-joints to consider the possible joint strength reduction resulted from the HAZ.

2.3. Parametric study

The parametric study covers steel grades of S460, S700, S900 and S1100, and 81 joint configurations without chord preloads were modelled for each steel grade. The chord diameter (d) was 480 mm, and analysed ratios (2γ) of chord diameter to wall thickness were 10, 15, 20, 25, 30, 35, 40, 45 and 50. The examined ratios (β) of brace to chord diameter were 0.2, 0.3, 0.4, 0.5, 0.6, 0.7, 0.8, 0.9 and 1.0. The values of brace and chord wall thickness were the same. The brace length (L_1) was set to be $2d_1$ to avoid the brace flexural buckling [20]. The chord length (L) was taken as $2(2\gamma/10)d+d_1$ with a minimum of $5d+d_1$. The chord length was determined in line with the minimum distance between the closest chord crown and an open chord end not connected to other members specified in prEN 1993-1-8 [21]; otherwise, the chord end shall be welded to a cap plate with a thickness of at least $1.5t$ for shorter chord length. The analysed parameter ranges were $0.2 \leq \beta \leq 1.0$ and $10 \leq 2\gamma \leq 50$. The material parameters and engineering stress-strain curves (see Fig. 7) which were adopted by Lan et al. [13] were employed for the FE simulations. Table 3 shows the material parameters used.

The validation study described in Section 2.1 of this paper shows that the constructed FE model without weld modelling can produce accurate prediction of the structural behaviour of CHS T-joints. Thus, the developed FE model was adopted without modelling the physical appearance of fillet welds in the subsequent simulations. This is to provide conservative strength prediction for CHS T-joints which may use butt welds with smaller weld leg sizes in practice. A suitable mesh size of 16 mm which was determined by a mesh convergence study was adopted. Similar to the boundary conditions employed for the validation study, the degrees of freedom of all nodes at each chord end were firstly coupled to a concentric reference point at the cross-section centre of each chord end and then only the translation along the chord axial direction and the in-plane rotation were allowed. All degrees of freedom at the brace end were restricted, except for the brace axial translation. Results of the parametric study herein and reported tests [14] were used to evaluate current design provisions and to propose design rules for HSS CHS T-joints.

3. Evaluation of design rules

3.1. Current design rules

The IIW recommendations [22, 23] are widely adopted by international design codes and guides for normal strength steel CHS joints. The CIDECT design guide [6] is based on the third edition of IIW recommendations [23] which employs the indentation limit of 3%*d*. The current Eurocode EN 1991-1-8 [7] adopts the second edition of IIW recommendations [22] which takes the peak loads as the joint strengths; however, the latest version of Eurocode prEN 1993-1-8 [21] is updated mainly in accordance with the third edition of IIW recommendations [23]. Background of the updated design rules for CHS joints is elaborated by van der Vegte et al. [24]. The representative CIDECT design rules will therefore be subsequently examined.

The CIDECT design strength equations for chord plastification in normal strength steel CHS T-joints under brace axial compression are as follows [6]:

$$N_{\mathrm{CIDECT,Rd}} = 2.6\left(1+6.8\beta^2\right)\gamma^{0.2}Q_{\mathrm{f}}\frac{f_{\mathrm{y}}t^2}{\sin\theta} \tag{1}$$

$$Q_{\mathrm{f}} = \left(1-|n|\right)^C \tag{2}$$

$$C=\begin{cases}0.45-0.25\beta & \text{for } n<0\\ 0.20 & \text{for } n\geq 0\end{cases} \tag{3}$$

$$n = \frac{N_0}{N_{\mathrm{pl,0}}}+\frac{M_0}{M_{\mathrm{pl,0}}} \quad \text{in the connecting face} \tag{4}$$

where Q_{f} is the chord stress equation which accounts for the effect of chord longitudinal stresses, and

n is the chord stress ratio defined as the sum of the ratio ($N_0/N_{pl,0}$) of the chord axial force (N_0) to the chord axial yield capacity ($N_{pl,0}$) and the ratio ($M_0/M_{pl,0}$) of the chord bending moment (M_0) to the chord plastic moment capacity ($M_{pl,0}$). Negative and positive values of n denote chord compression and tension stresses, respectively.

The CIDECT design strength equations are converted from the CIDECT mean strength equations which are based on the regression analysis of FE data of S355 CHS T-joints, and the CIDECT mean strength equation is as follows [24]:

$$N_{\text{CIDECT,Mean}} = 3.1\left(1+6.8\beta^2\right)\gamma^{0.2}Q_{\text{f}}\frac{f_{\text{y}}t^2}{\sin\theta} \tag{5}$$

An implicit safety factor of 1.19 is incorporated in Eq. (1) when compared with Eq. (5). The validity ranges of the design and mean strength equations for the CHS T-joints are $0.2\leq\beta\leq1.0$ and $2\gamma\leq50$, and the chord cross-section should be class 1 or 2 for the chord under compression. It should be noted that the static strength of simply supported CHS T-joints under brace axial compression is governed by a combination of (local) joint failure and failure because of the global chord bending moment which is resulted from the applied brace force. The CIDECT mean strength equation with Q_f=1.0 (see Eq. (5)) is developed for CHS T-joints with zero global chord bending moment at the chord crown in order to provide the baseline equation for CHS T-joints [25]. This is achieved by applying the compensating bending moment at each chord end to eliminate the global chord bending moment at the chord crown in simply supported CHS T-joints. The effect of the global chord bending moment and the applied chord axial force and chord bending moment (i.e. chord preloads) on the joint strength can be quantified by the chord stress function (Q_f).

3.2. Assessment of the CIDECT design rules

This subsection examines the suitability of the current CIDECT mean strength equation (Eq. (5)) for HSS CHS T-joints. The CIDECT mean strength prediction ($N_{\text{CIDECT,Mean}}$) was evaluated against the test strength (N_{Test}) reported by Lan et al. [14] and FE strength (N_{FE}) obtained in Section 2.3 of this paper. It should be noted that for the analysed test and FE specimens, there were no applied chord preloads in the simply supported CHS T-joints. However, the global chord bending moment (M_0) at the chord crown resulted from the applied brace axial compression should be considered in the calculation of Q_f using Eqs. (2-4). The value of M_0 can be approximated by $M_0=N_f(L_s-d_1)/4$, where N_f is the joint strength obtained from the tests and FE simulations, L_s is the distance between the centres of two supports at the chord ends and d_1 is the brace diameter. The chord stress ratio (n) varied from -0.22 to -0.48 for the test specimens listed in Table 1 and ranged from -0.18 to -1.24 for the FE specimens described in Section 2.3 of this paper. The absolute value of n becomes larger for larger β ratio and smaller 2γ ratio indicating that the global chord bending moment (M_0) becomes more dominating in the failure of simply supported CHS T-joints. The chord member failure instead of joint failure occurs for $n\leq-1$. The joint specimens with $n>-1$ which failed by chord plastification were included in the subsequent analysis.

The comparison of CIDECT mean strengths ($N_{CIDECT,Mean}$) with FE strengths (N_{FE}) for HSS CHS T-joints failing by chord plastification is illustrated in Fig. 10. Table 4 summarizes the mean values and coefficients of variation (COV) of $N_{FE}/N_{CIDECT,Mean}$ ratio for HSS CHS T-joints. The mean values of $N_{FE}/N_{CIDECT,Mean}$ ratio for steel grades S460, S700, S900 and S1100 are 1.01, 0.84, 0.68 and 0.63 with corresponding COV of 0.127, 0.171, 0.241 and 0.271. It is shown that the $N_{FE}/N_{CIDECT,Mean}$ ratio generally decreases for higher steel grades and larger 2γ ratio, and the effect of β ratio on the $N_{FE}/N_{CIDECT,Mean}$ ratio is relatively insignificant. The CIDECT mean strength prediction is slightly unconservative for S460 CHS T-joints and becomes increasingly unconservative and scattered for steel grades greater than S460 and larger 2γ ratio. The obtained FE results (see Fig. 10(c)) also coincide with the reported test results summarised in Table 1. The mean value and COV of $N_{Test}/N_{CIDECT,Mean}$ ratio for CHS T-joints with a nominal yield stress of 960 MPa are 0.50 and 0.066, respectively. The CIDECT mean strength prediction is very unconservative for the test specimens with large 2γ ratio ranging from 42.8 to 54.2.

The applied brace axial compression is mainly resisted by the bending action of the chord characterised by the localised indentation at the brace-chord intersection and global bending deflection of the chord in simply supported CHS T-joints. Fig. 11 shows representative load-indentation curves of HSS CHS T-joints. Fig. 12 further illustrates the typical yielding patterns of HSS CHS T-joints with β=0.4 and 2γ=25 at the determined joint strengths. The highly strained areas in red colour became plastic. It is shown that the joint strength of S460 CHS T-joints is generally determined by the peak load or the load at the indentation limit of 3%d which is close to the peak load (i.e. largely strength-controlled). Large inelastic deformation (see Fig. 11) and extensive yielding (see Fig. 12(a)) occur at the indentation limit. This therefore indicates that the adopted indentation limit is not a governing factor limiting the joint strength, and the yield stress of HSS can be utilised effectively. The corresponding CIDECT mean strength equation (Eq. (5)) is thus relatively accurate. However, the joint strength is mostly taken as the load at the indentation limit (i.e. deformation controlled) for steel grades greater than S460 and large 2γ ratios. The strength reserve (R) defined as the ratio of the peak load to the load at the indentation limit is larger for higher steel grades and larger 2γ ratio. The mean values of R are 1.01, 1.07, 1.17 and 1.26 for steel grades S460, S700, S900 and S1100, respectively in the parametric study and 1.35 for the test specimens with a nominal yield stress of 960 MPa and large 2γ ratios ranging from 42.8 to 54.2 (see Table 1). The corresponding deformation and stresses at the brace-chord intersection of the joint at the indentation limit is largely elastic (see Figs. 11-12). The adopted indentation limit becomes the governing factor limiting the joint strength. Therefore, the yield stress of HSS cannot be utilised effectively and the corresponding CIDECT mean strength prediction is more unconservative.

4. Proposed design rules

4.1. Proposed mean strength equation

The CIDECT mean strength equation (Eq. (5)) for normal strength steel CHS T-joints was modified and extended for their HSS counterparts. The analysis in Section 3.2 of this paper demonstrates that the improved yield stress of HSS cannot be fully utilised for higher steel grade and larger 2γ ratio, and the corresponding CIDECT mean strength prediction is unconservative and scattered. It is thus suggested to tighten the range of 2γ ratio to be within 40 for steel grades ranging from S460 to S700 and not greater than 30 for steel grades higher than S700 up to S1100. The CIDECT design guide [6] imposes that the chord cross-section under compression should be class 1 or 2 in order to achieve the plastic moment capacity ($M_{\mathrm{pl,0}}$) used in Eq. (4) for the chord. The plastic slenderness limits i.e. maximum diameter to wall thickness ratios for S460, S700, S900 and S1100 CHS tubes are 54, 44, 37 and 35, respectively [26] which are larger than the corresponding proposed limits of 2γ ratio. Additional check of chord cross-section classification is therefore not needed for the recommended 2γ ratio. The effect of β ratio on the $N_{\mathrm{FE}}/N_{\mathrm{CIDECT,Mean}}$ ratio is relatively insignificant, and thus the CIDECT validity range of $0.2\leq\beta\leq1.0$ is suggested. The suggested ranges of 2γ and β ratios can avoid applying small reduction factors of joint strength to the CIDECT mean strength equation for HSS CHS T-joints which largely eliminate the benefits of using HSS.

The CIDECT mean strength prediction is generally unconservative for HSS CHS T-joints when β and 2γ ratios are within the recommended limits (see Fig. 11) because of the adopted indentation limit. Mean strength equations for CHS T-joints in steel grades varying from S460 to S1100 were proposed as follows:

$$N_{\mathrm{Proposed,Mean}} = 3.1\left(1+6.8\beta^2\right)\gamma^{0.2}Q_{\mathrm{y}}Q_{\mathrm{f}}\frac{f_{\mathrm{y}}t^2}{\sin\theta} \tag{6}$$

$$Q_{\mathrm{y}} = 1.1-62f_{\mathrm{y}}/E \tag{7}$$

where Q_{y} is the proposed reduction factor to account for the under-utilisation of HSS and equals to 0.95, 0.88, 0.79 and 0.75 for the examined steel grades S460, S700, S900 and S1100, respectively. It is noted that Q_{y}=1.0 for S355 CHS T-joints and the proposed mean strength equation (Eq. (6)) is the same as the CIDECT mean strength equation (Eq. (5)) for S355 CHS T-joints. The validity ranges of the proposed mean strength equations are $0.2\leq\beta\leq1.0$ for steel grades from S460 to S1100, $2\gamma\leq40$ for steel grades from S460 to S700 and $2\gamma\leq30$ for steel grades greater than S700 up to S1100.

The proposed mean strength equation (Eq. (6)) was assessed against the FE results obtained in this study. The FE specimens with joint parameter ranges beyond the suggested limits were excluded for the analysis. Fig. 13 shows the comparison of the mean strengths ($N_{\text{Proposed,Mean}}$) calculated using Eqs. (6-7) with the FE strengths (N_{FE}). Table 4 summarises the results of statistical analysis for the $N_{\text{FE}}/N_{\text{Proposed,Mean}}$ ratio. The mean values of the $N_{\text{FE}}/N_{\text{Proposed,Mean}}$ ratio for steel grades S460, S700, S900 and S1100 are 1.12, 1.02, 1.04 and 1.03 with corresponding COV of 0.102, 0.135, 0.146 and 0.170. The mean value and COV of the $N_{\text{FE}}/N_{\text{Proposed,Mean}}$ ratio for the four steel grades are 1.06 and 0.141, respectively. The proposed mean strength equation can produce reasonably conservative and consistent strength prediction for S460 CHS T-joints. The mean strength prediction is more accurate and consistent for CHS T-joints in steel grades S700, S900 and S1100 when compared with the CIDECT mean strength prediction. It is noted that the proposed reduction factor of joint strength (Q_{y}) could be conservative for smaller 2γ ratio and unconservative for larger 2γ ratio (see Fig. (13)).

4.2. Determination of design strengths

The IIW recommendations [22, 23] adopted a two-step procedure to convert the mean strength equation ($N_{\text{u,m}}$) derived using the regression analysis of test and FE results to the design strength equation ($N_{\text{u,Rd}}$). The mean strength equation was firstly converted to the characteristic strength equation ($N_{\text{u,k}}$) by considering the fabrication tolerance, mean value and scatter of data, and a correction factor of yield stress. The design strength equation was then derived from the characteristic strength equation divided by a suitable partial safety factor. The IIW procedure of converting mean to design strength equations is elaborated by van der Vegte et al. [24] and is adopted herein. The characteristic strength is obtained from [24]:

$$N_{\text{u,k}} = N_{\text{u,m}}(1-1.64V_{\text{N}_\text{u}})\frac{f_{\text{y,m}}}{f_{\text{y,k}}} \tag{8}$$

$$V_{N_u} = \frac{[\mathrm{VAR}(N_u)]^{0.5}}{N_u} \tag{9}$$

$$\mathrm{VAR}(N_u) = N_u^2\left[(\frac{s_{f_y}}{f_y})^2 + (1.8\frac{s_t}{t})^2 + (\frac{s_\delta}{\delta})^2\right] \tag{10}$$

where the mean to design yield stress ratio $f_{y,m}/f_{y,k}$=1/0.85, and the standard deviations of yield stress of the chord (s_{fy}/f_y) and chord wall thickness (s_t/t) were taken as 0.075 and 0.05, respectively [24]. The mean value and COV of 145 CHS T-joints summarised in Table 4 were adopted (i.e. mean=1.06 and s_δ/δ=0.141). The characteristic strength followed by a correction of the mean value is obtained [24]:

$$N_{u,k} = (1-1.64\times 0.18)/0.85\times 1.06N_{u,m} = 0.88N_{u,m} \tag{11}$$

The chord plastification in HSS CHS T-joints is a ductile failure mode, and the deformation capacity of CHS T-joints with a nominal yield stress of 960 MPa could be considered as reasonably sufficient [14]. A partial safety factor (γ_m) of 1.1 adopted by the CIDECT design guide [6] for normal strength steel CHS T-joints is thus suggested for their HSS counterparts, and the design strength is as follows:

$$N_{u,Rd} = \frac{N_{u,k}}{\gamma_m} = 0.80N_{u,m} \tag{12}$$

The design strength equation for chord plastification in CHS T-joints using steel grades from S460 to S1100 is as follows:

$$N_{u,Rd} = 2.48\left(1+6.8\beta^2\right)\gamma^{0.2}Q_y Q_f \frac{f_y t^2}{\sin\theta} \tag{13}$$

The design strength calculated using Eq. (13) is 5% lower than the corresponding CIDECT design strength obtained from Eq. (1) for S355 CHS T-joints. The strength reserve defined by the ratio of the peak load to the load at the indentation limit which was taken as the joint strength for the most of HSS CHS T-joints is large as discussed in Section 3.2 of this paper. The same CIDECT design strength equation modified by the proposed reduction factor is thus suggested for HSS CHS T-joints in order to be more user-friendly as follows:

$$N_{\mathrm{Proposed,Rd}} = 2.6\left(1+6.8\beta^2\right)\gamma^{0.2}Q_y Q_f \frac{f_y t^2}{\sin\theta} \tag{14}$$

It is noted that the range of 2γ ratio for the proposed mean and design strength equations is suggested to be tightened to allow for more effective use of the improved yield stress of HSS. Reinforcing methods can be employed in HSS CHS T-joints for the use of commercially available HSS CHS tubes with 2γ ratio beyond the recommended limits, e.g. grouting concrete [27] and welding internal ring stiffeners [28, 29] and external stiffeners [30]. Studies on HSS reinforced tubular joints are needed. It should also be noted that high strength steel often exhibits lower material ductility, and this sparks the concern of the insufficient deformation capacity of HSS tubular joints. The deformation capacity of CHS T-joints with a nominal yield stress of 960 MPa were demonstrated to be sufficient for the loading of brace axial compression [14]; however, tests which examine the deformation capacity and joint strength for other loading cases such as brace axial tension remain limited. The current CIDECT design guide [6] adopts the same design rules for CHS T-joints under brace axial compression and tension. The applicability of the proposed design rules in this study for brace axial tension needs to be further verified.

5. Conclusions

The structural behaviour and static strength of HSS CHS T-joints under brace axial compression were investigated. FE analysis was carried out covering a wide range of geometric parameters and steel grades ranging from S460 to S1100. The β ratio ranged from 0.2 to 1.0 and 2γ ratio varied from 10 to 50. The chord plastification failure of HSS CHS T-joints was examined. The effect of HAZ on the joint behaviour and influences of the steel grade, β ratio and 2γ ratio on the suitability of the CIDECT mean strength equations for HSS CHS T-joints were evaluated. Design rules were proposed for HSS CHS T-joints. The conclusions are summarized as follows:

(1) The effect of HAZ on the initial stiffness of HSS CHS T-joints is found to be insignificant. The material softening in HAZ can lower the joint strength; however, the joint strength reduction is less pronounced.

(2) The CIDECT mean strength prediction is relatively accurate for S460 CHS T-joints and becomes

increasingly unconservative for higher steel grades and larger 2γ ratio. The influence of β ratio on the suitability of the CIDECT mean strength equations is minor.

(3) The CIDECT mean strength prediction for HSS CHS T-joints is unconservative because the improved yield stress of HSS, in general, cannot be effectively utilised. The under-utilisation of HSS is due to the adopted CIDECT indentation limit.

(4) The suggested ranges of joint parameters are $0.2 \leq \beta \leq 1.0$ for steel grades ranging from S460 to S1100, $2\gamma \leq 40$ for steel grades varying from S460 to S700 and $2\gamma \leq 30$ for steel grades greater than S700 up to S1100 to allow for more effective use of HSS.

(5) Mean and design strength equations modified from the CIDECT strength equations were proposed for HSS CHS T-joints with 2γ and β ratios which are within the suggested ranges.

References

[1] X.Y. Lan, T.M. Chan, B. Young, Structural behaviour and design of high strength steel RHS X-joints, Eng. Struct. 200 (2019) 109494.

[2] X.Y. Lan, J.B. Chen, T.M. Chan, B. Young, The continuous strength method for the design of high strength steel tubular sections in compression, Eng. Struct. 162 (2018) 177-187.

[3] X.Y. Lan, J.B. Chen, T.M. Chan, B. Young, The continuous strength method for the design of high strength steel tubular sections in bending, J. Constr. Steel Res. 160 (2019) 499-509.

[4] J.L. Ma, T.M. Chan, B. Young, Design of cold-formed high-strength steel tubular stub columns, J. Struct. Eng. 144(6) (2018) 04018063.

[5] J.A. Packer, J. Wardenier, X.L. Zhao, G.J. van der Vegte, Y. Kurobane, Design Guide for Rectangular Hollow Section (RHS) Joints Under Predominantly Static Loading, CIDECT, Verlag TUV Rheinland, Cologne, Germany, 2009.

[6] J. Wardenier, Y. Kurobane, J.A. Packer, G.J. van der Vegte, X.L. Zhao, Design Guide for Circular Hollow Section (CHS) Joints under Predominantly Static Loading, CIDECT, Verlag TUV Rheinland, Cologne, Germany, 2008.

[7] Eurocode 3 (EC3), Design of Steel Structures-Part 1-8: Design of Joints. European Committee for Standardization, EN 1993-1-8, CEN, Brussels, 2005.

[8] EN 1993-1-12, Eurocode 3: Design of Steel Structures-Part 1–12: Additional Rules for the Extension of EN 1993 up to Steel Grades S700, European Committee for Standardization, EN 1993-1-12, CEN, Brussels, 2007.

[9] X.Y. Lan, T.M. Chan, Recent research advances of high strength steel welded hollow section joints, Struct. 17 (2019) 58-65.

[10] R. Puthli, O. Bucak, S. Herion, O. Fleischer, A. Fischl, O. Josat, Adaptation and extension of the valid design formulae for joints made of high-strength steels up to S690 for cold-formed and hot-rolled sections, CIDECT Report 5BT-7/10 (Draft Final Report), CIDECT, Germany, 2011.

[11] C.H. Lee, S.H. Kim, D.H. Chung, D.K. Kim, J.W. Kim, Experimental and numerical study of cold-formed high-strength steel CHS X-joints, J. Struct. Eng. 143 (8) (2017), 04017077.

[12] X.Y. Lan, T.M. Chan, B. Young, Static strength of high strength steel CHS X-joints under axial compression, J. Constr. Steel Res. 138 (2017) 369–379.

[13] X.Y. Lan, T.M. Chan, B. Young, Structural behaviour and design of chord plastification in high strength steel CHS X-joints, Constr. Build. Mater. 191 (2018), 1252-1267.

[14] X.Y. Lan, T.M. Chan, B. Young, Experimental study on the behaviour and strength of high strength steel CHS T- and X-joints, Eng. Struct. 206 (2020) 110182.

[15] Abaqus/Standard. Version 6.13-1. USA: K. a. S. Hibbit; 2013.

[16] R. Stroetmann, Thoralf Kastner, A. Halsig, P. Mayr, Mechanical properties and a new design approach for welded joints at high strength steels, Engineering Research and Practice for Steel Construction, Hong Kong 2018, pp. 79–90.

[17] J. Siltanen, S. Tihinen, J. Kömi, Laser and laser gas-metal-arc hybrid welding of 960 MPa direct-quenched structural steel in a butt joint configuration, J. Laser Appl. 27(S2) (2015) S29007.

[18] F. Javidan, A. Heidarpour, X.L. Zhao, C.R. Hutchinson, J. Minkkinen, Effect of weld on the mechanical properties of high strength and ultra-high strength steel tubes in fabricated hybrid sections, Eng. Struct. 118 (2016) 16–27.

[19] J.L. Ma, T.M. Chan, B. Young, Material properties and residual stresses of cold-formed high strength steel hollow sections, J. Constr. Steel Res. 109 (2015) 152–165.

[20] X.Y. Lan, Y Huang, Structural design of cold-formed stainless steel tubular X- and T-joints at elevated temperatures, Thin Wall. Struct. 108 (2016) 270-279.

[21] Eurocode 3 (EC3), Design of Steel Structures-Part 1-8: Design of Joints. European Committee for Standardization, prEN 1993-1-8, CEN, Brussels, 2018.

[22] International Institute of Welding (IIW) Subcommission XV-E, IIW Doc. XV-701-89: Design recommendations for hollow section joints–predominantly statically loaded, 2nd Ed., IIW, Paris, 1989.

[23] International Institute of Welding (IIW) Subcommission XV-E, IIW Doc. XV-1329-09: Static Design Procedure for Welded Hollow Section Joints–Recommendations, 3rd Ed., IIW, Singapore, 2009.

[24] G.J. van der Vegte, J. Wardenier, X.L. Zhao, J.A. Packer, Evaluation of new CHS strength formulae to design strengths, Tubular Structures XII, CRC Press, London 2009, pp. 313–322.

[25] G.J. van der Vegte, Y. Makino, Ultimate strength formulation for axially loaded CHS uniplanar T-joints, The 15th International Offshore and Polar Engineering Conference, Seoul 2005, pp. 279-286.

[26] J.L. Ma, T.M. Chan, B. Young, Design of cold-formed high strength steel tubular beams, Eng. Struct. 151 (2017) 432–443.

[27] H.T. Li, B. Young, Experimental Investigation of Concrete-Filled High-Strength Steel Tubular X Joints, J. Struct. Eng. 144(10) (2018) 04018178.

[28] X.Y. Lan, F. Wang, C. Ning, X.F. Xu, X.R. Pan, Z.F. Luo, Strength of internally ring-stiffened tubular DT-joints subjected to brace axial loading, J. Constr. Steel Res. 125 (2016) 88–94.

[29] X.Y. Lan, F. Wang, Z.F. Luo, D.D. Liu, C. Ning, X.F. Xu, Joint strength reduction factor of internally ring-stiffened tubular joints at elevated temperatures, Adv. Struct. Eng. 19(10) (2016) 1650–1660.

[30] W. Li, S. Zhang, W. Huo, Y. Bai, L. Zhu, Axial compression capacity of steel CHS X-joints strengthened with external stiffeners, J. Constr. Steel Res. 141 (2018) 156–166.

Table 1

Measured dimensions of cold-formed HSS CHS T-joint specimens tested by Lan et al. [14].

Specimen	d (mm)	t (mm)	L (mm)	d_1 (mm)	t_1 (mm)	L_1 (mm)	w (mm)	L_s (mm)	β	2γ	f_y (MPa)	N_{Test} (kN)	N_{Test}/N_{CIDECT}	N_{Test}/N_{FE}
T1	251.7	4.68	1590	234.9	4.73	469	5.5	1500	0.93	53.8	972	413	0.54	1.01
T1#	251.8	4.65	1590	235.0	4.67	464	6.2	1500	0.93	54.1	972	389	0.51	0.95
T2	251.4	4.64	1590	217.2	4.66	432	6.1	1500	0.86	54.2	972	343	0.51	1.08
T3	251.0	4.75	1590	174.8	4.69	348	6.2	1500	0.70	52.9	972	238	0.46	1.09
T4	251.4	4.76	1590	151.1	4.72	300	7.3	1500	0.60	52.8	972	187	0.45	1.05
T5	203.5	4.76	1302	175.1	4.70	350	6.5	1212	0.86	42.8	1012	355	0.53	0.96
T6	235.4	4.72	1494	202.6	4.68	405	5.9	1404	0.86	49.9	990	350	0.51	0.99
Mean													0.50	1.02
COV													0.066	0.053

Note: # denotes repeated tests.

Table 2

Effects of heat affected zones on CHS T-joints using S900 and S1100 steel.

Specimen	d (mm)	t (mm)	d_1 (mm)	t_1 (mm)	β	2γ	Steel	N_{u1} (kN)	N_{u2} (kN)	N_{u2}/N_{u1}
T4	251.4	4.76	151.1	4.72	0.6	52.8	S900	187	182	0.98
							S1100	187	180	0.96
T4-1	251.4	14.00	151.1	8.40	0.6	18.0	S900	1937	1798	0.93
							S1100	2077	1866	0.90
T4-2	251.4	7.50	151.1	4.50	0.6	33.5	S900	539	519	0.96
							S1100	541	515	0.95
T4-3	251.4	7.50	75.4	4.50	0.3	33.5	S900	303	289	0.95
							S1100	307	288	0.94
T4-4	251.4	7.50	197.6	4.50	0.8	33.5	S900	792	757	0.96
							S1100	799	754	0.94

Note: N_{u1} and N_{u2} denote the static strengths of CHS T-joints without and with HAZ, respectively.

Table 3

Material parameters adopted for HSS CHS T-joints.

Steel	E (GPa)	f_y (MPa)	f_u (MPa)	ε_u (%)
S460	210	505	616	10.81
S700	214	772	816	4.64
S900	210	1054	1116	2.26
S900-R10	210	949	1004	2.26
S900-R20	210	843	893	4.75
S1100	207	1152	1317	2.20
S1100-R15	207	979	1119	2.20
S1100-R30	207	806	922	7.70

Note: The value following the letter R denotes the percentage of material strength reduction; ε_u is the ultimate strain at ultimate stress.

Table 4

Results of statistical analysis for HSS CHS T-joints.

Steel	$N_{FE}/N_{CIDECT,Mean}$			$N_{FE}/N_{Proposed,Mean}$		
	No. of data	Mean	COV	No. of data	Mean	COV
S460	61	1.01	0.127	43	1.12	0.102
S700	61	0.84	0.171	43	1.02	0.135
S900	66	0.68	0.241	30	1.04	0.146
S1100	65	0.63	0.271	29	1.03	0.170
Total	253	0.79	0.272	145	1.06	0.141

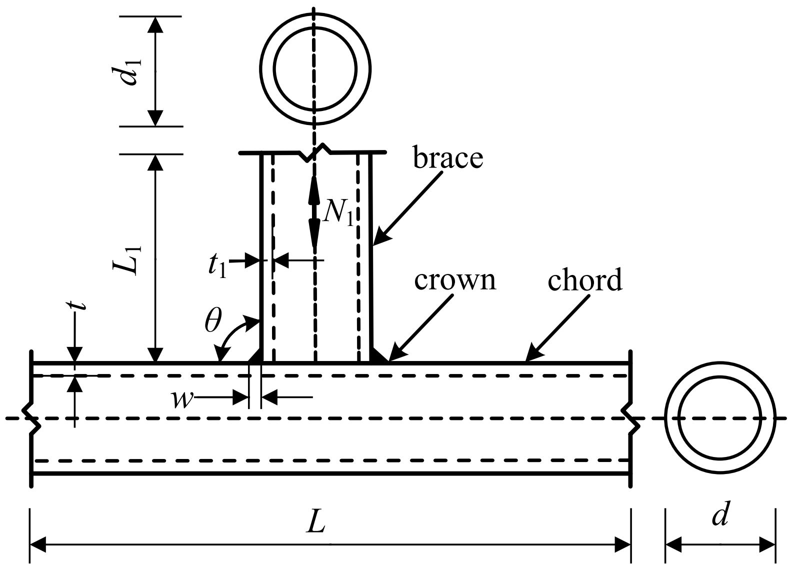

Fig. 1. Configuration and notations of CHS T-joints.

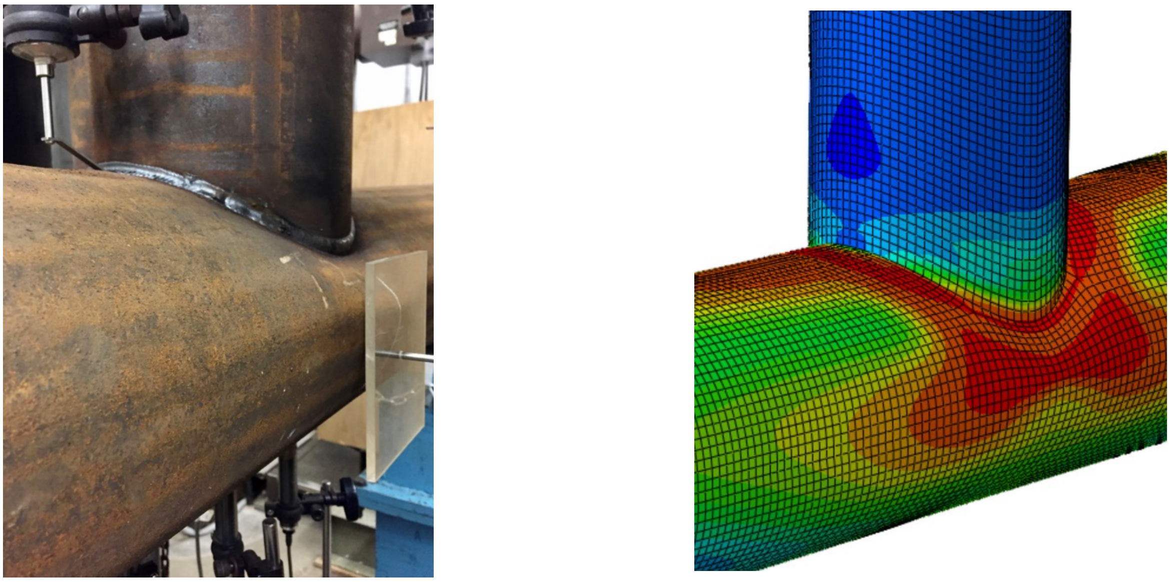

(a) Test observation (b) Numerical simulation

Fig. 2. Comparison of the failure mode of chord plastification in the T2 specimen [14].

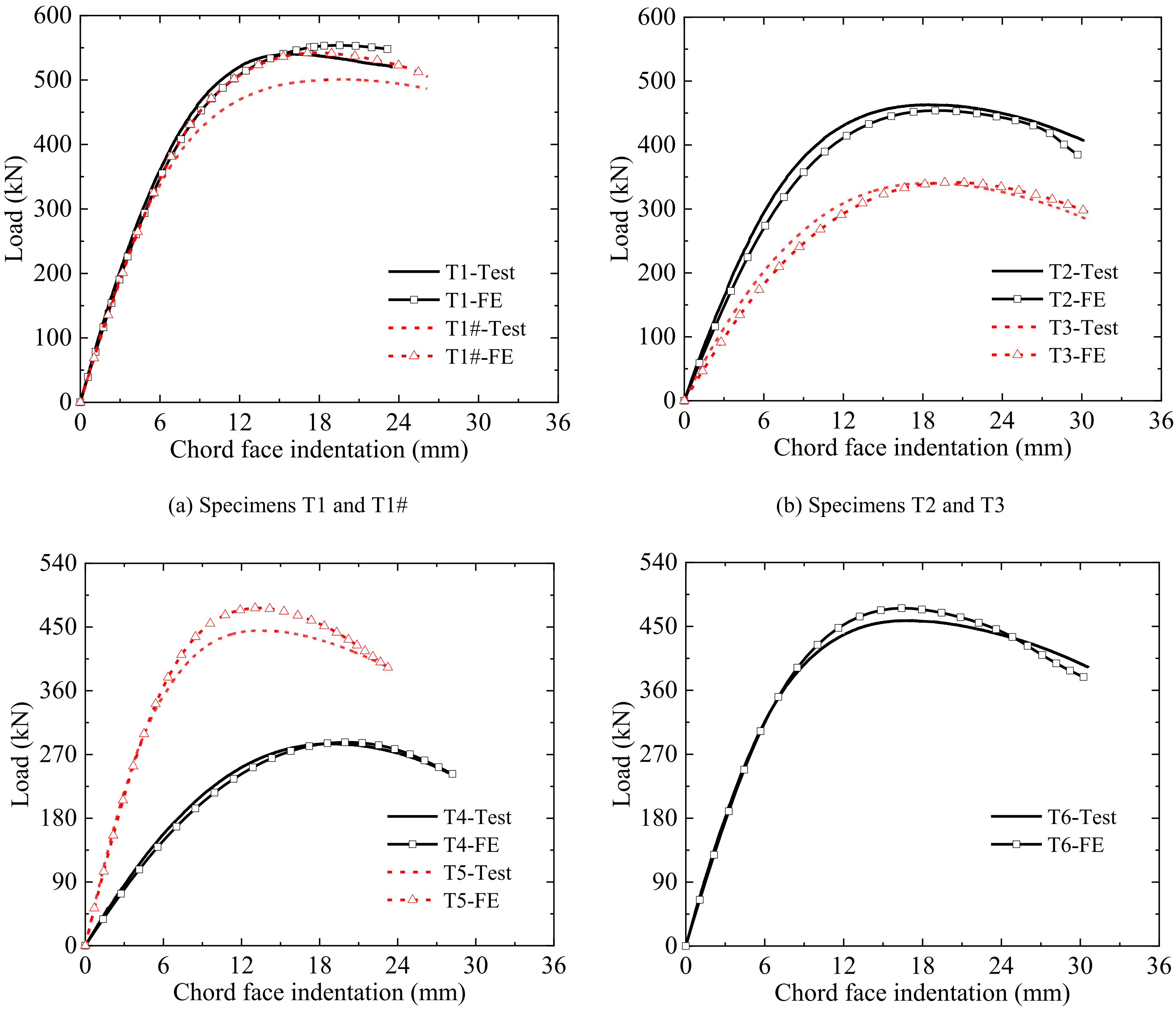

(a) Specimens T1 and T1#

(b) Specimens T2 and T3

(c) Specimens T4 and T5

(d) Specimen T6

Fig. 3. Comparison of load-chord face indentation curves of HSS CHS T-joint specimens.

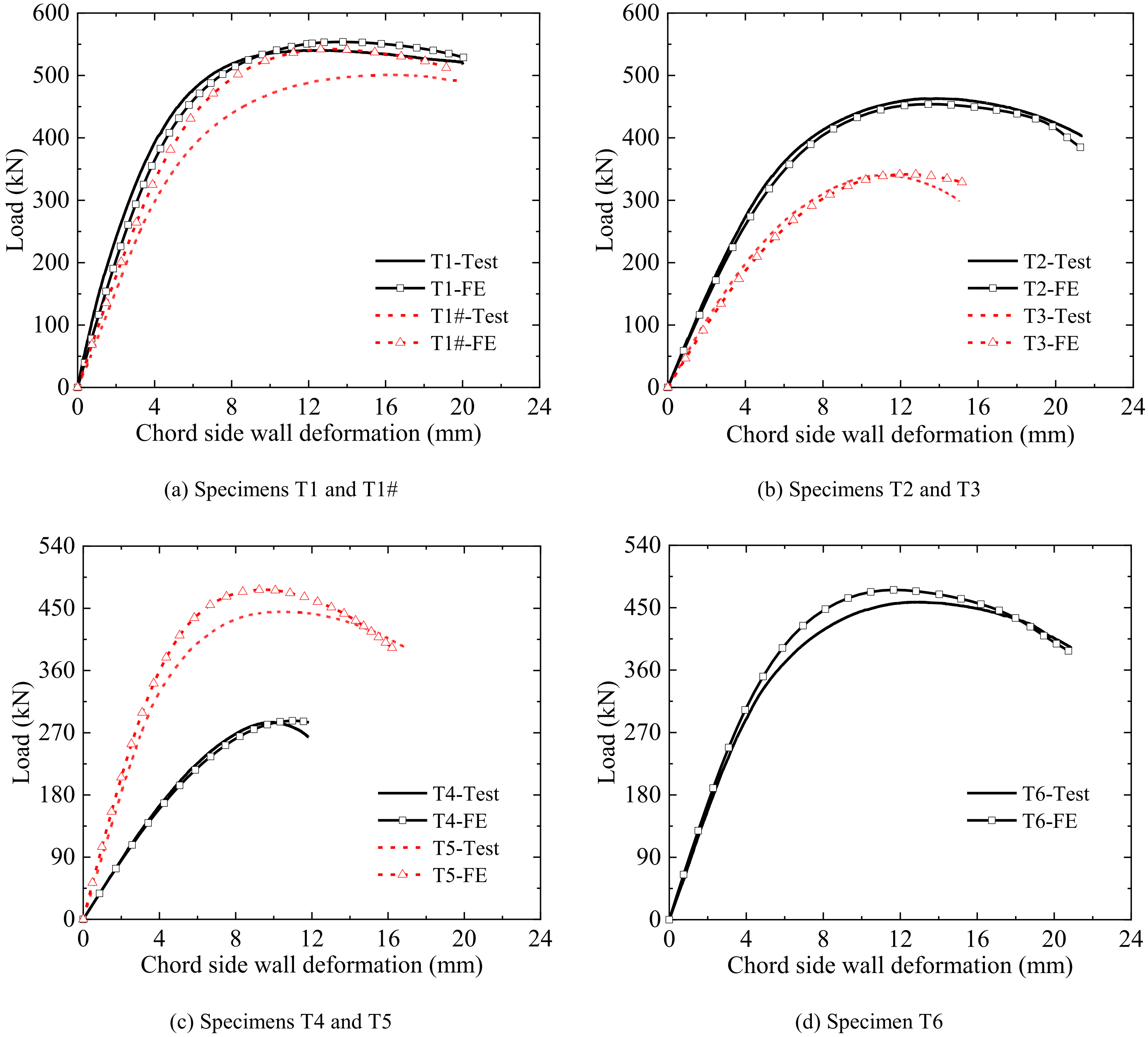

Fig. 4. Comparison of load-chord side wall deformation curves of HSS CHS T-joint specimens.

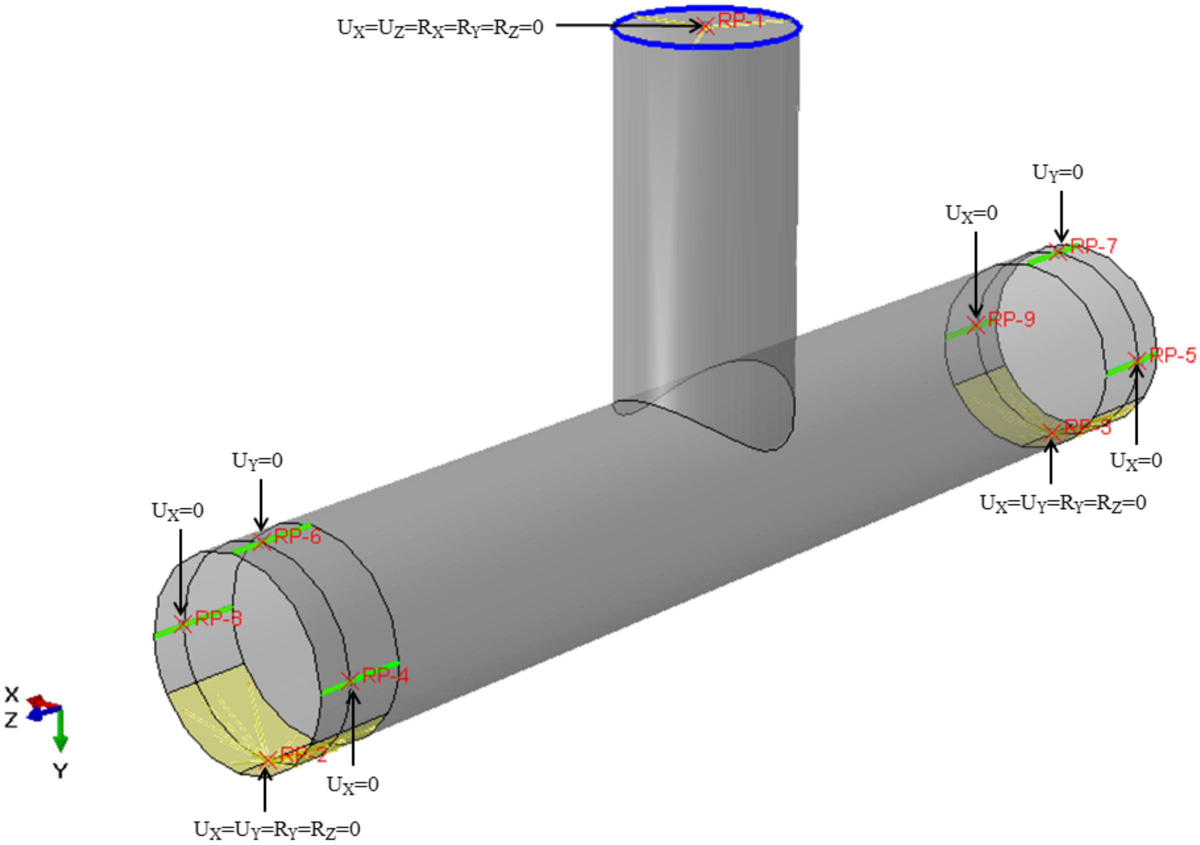

Fig. 5. Boundary conditions adopted for the validation of FE model.

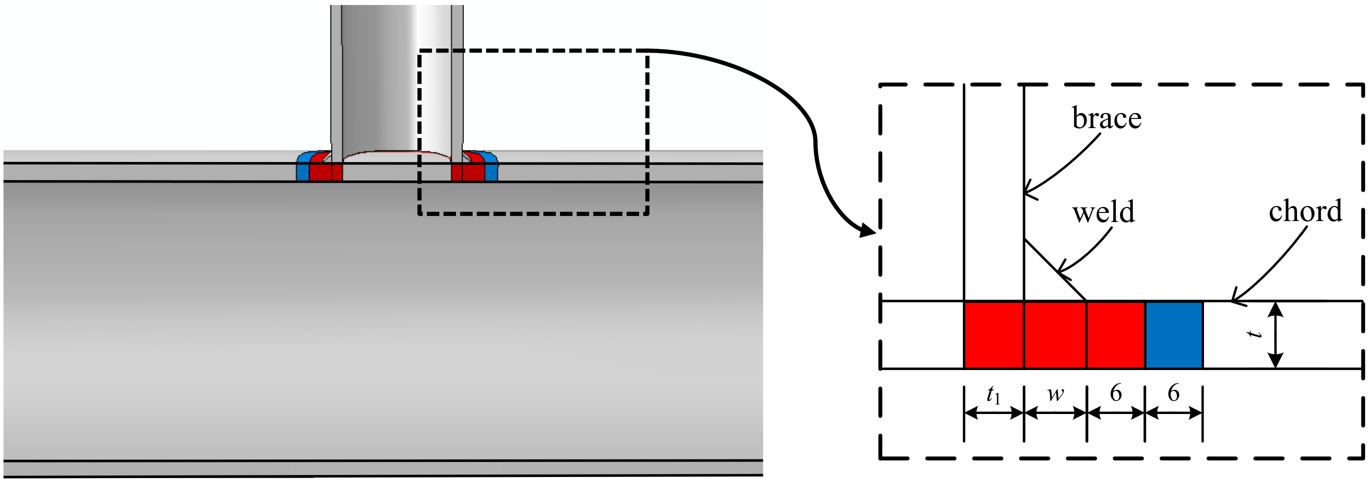

Fig. 6. Heat affected zones in S900 and S1100 CHS T-joints (dimensions in mm).

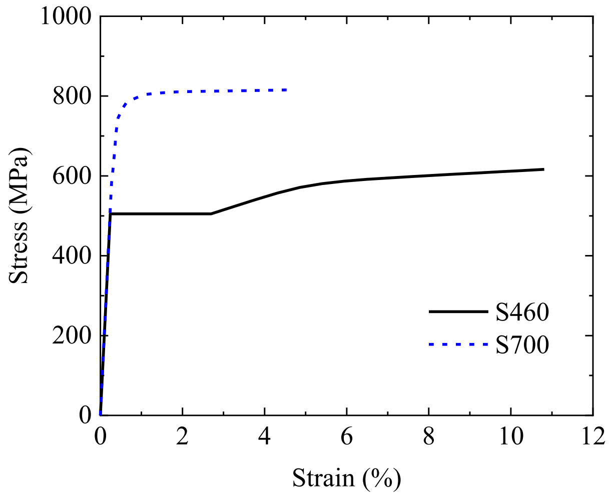

(a) S460 and S700

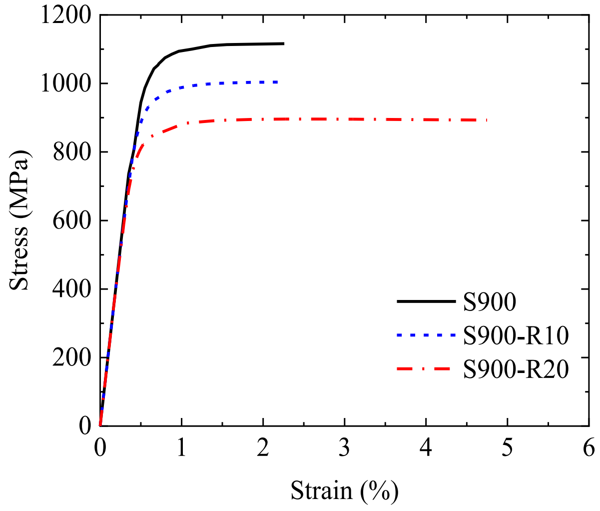

(b) S900

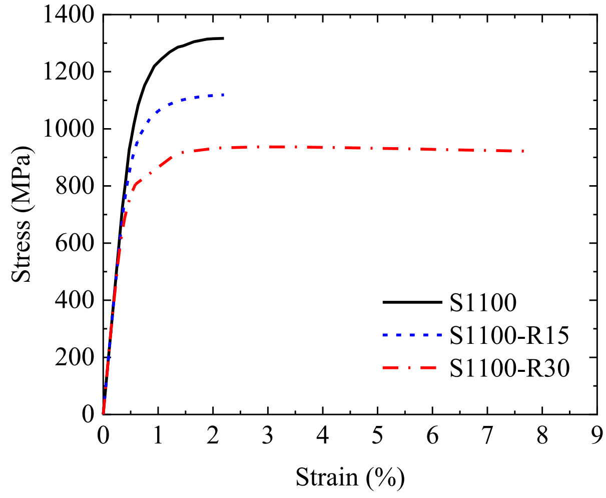

(c) S1100

Fig. 7. Engineering stress-strain curves of high strength steel (Lan et al. [13]).

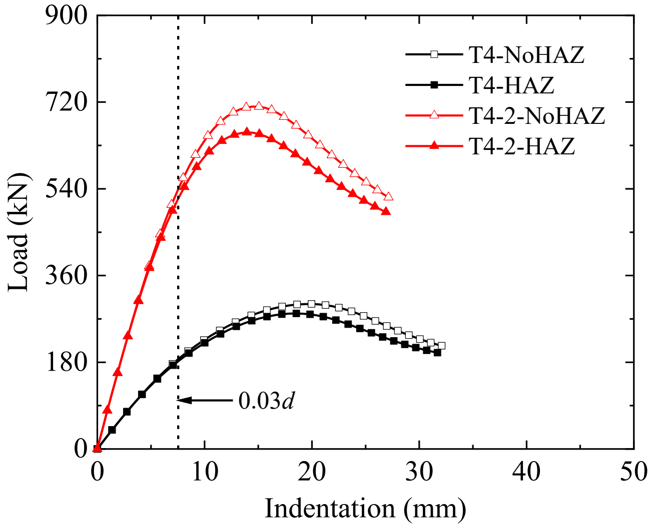

(a) FE specimens T4 and T4-2

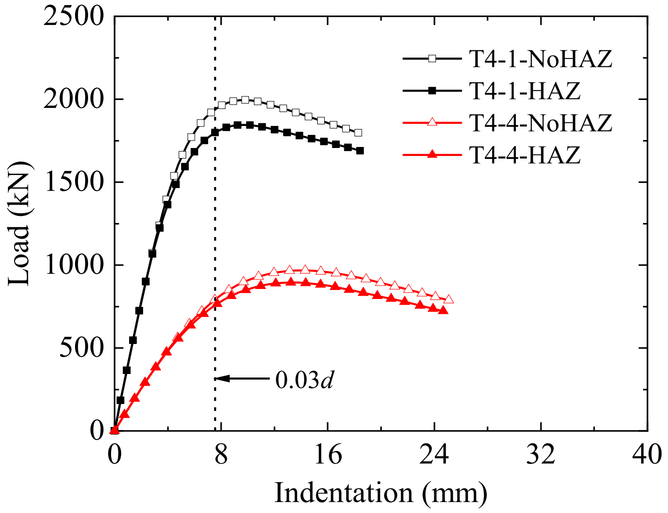

(b) FE specimens T4-1 and T4-4

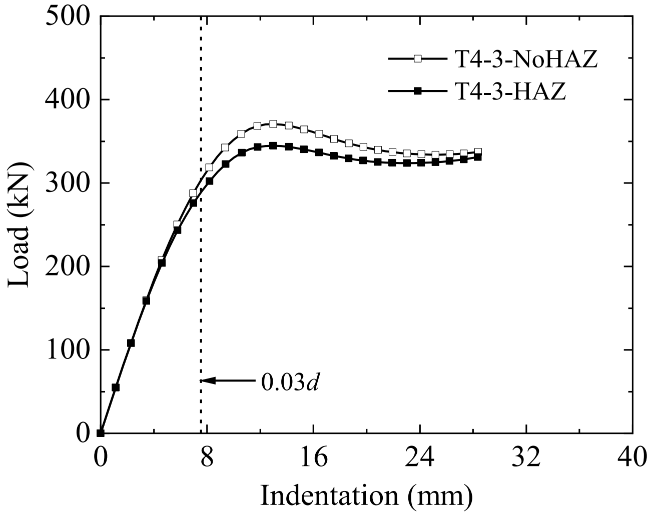

(c) FE specimen T4-3

Fig. 8. Load-indentation curves of S900 steel CHS T-joints without and with HAZ.

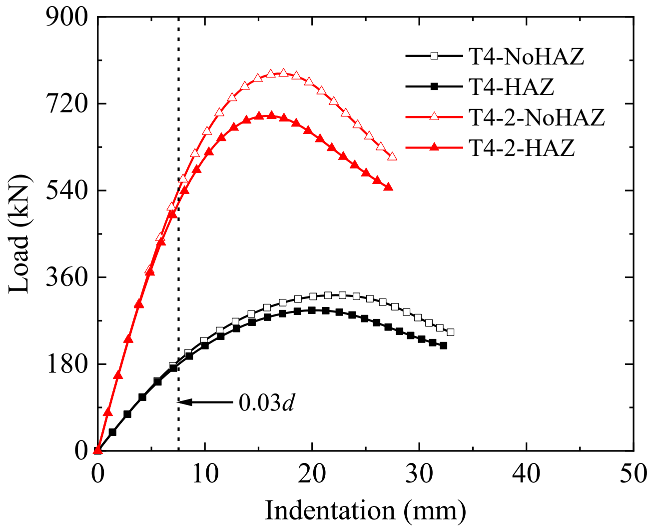

(a) FE specimens T4 and T4-2

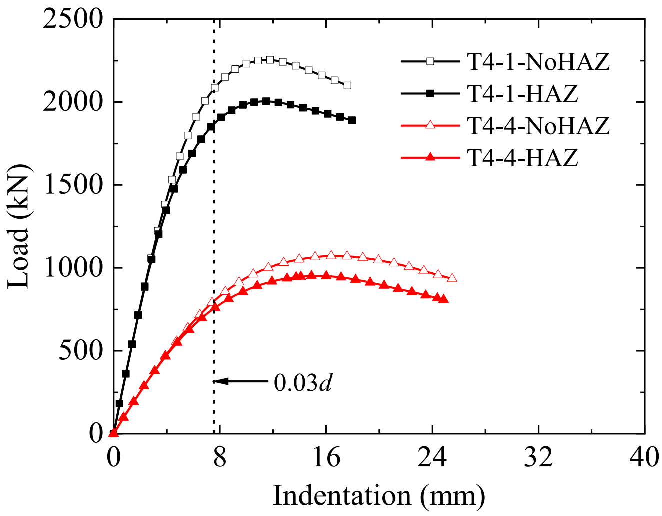

(b) FE specimens T4-1 and T4-4

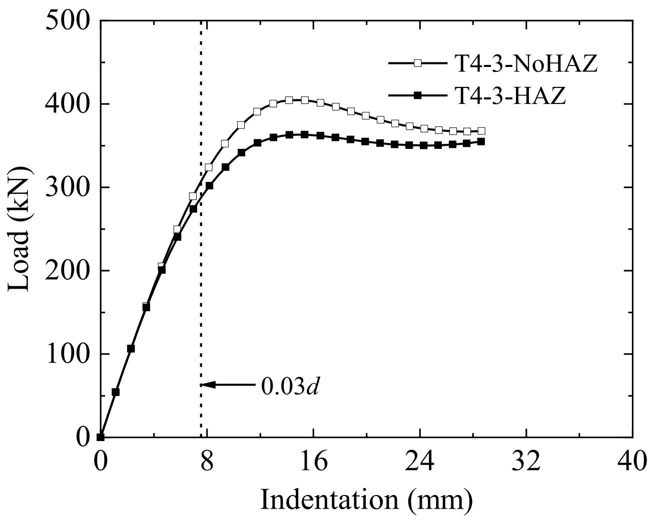

(c) FE specimen T4-3

Fig. 9. Load-indentation curves of S1100 steel CHS T-joints without and with HAZ.

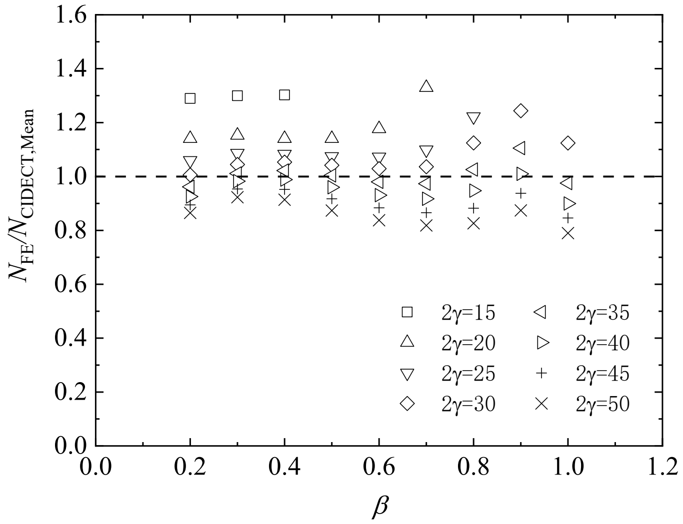

(a) S460

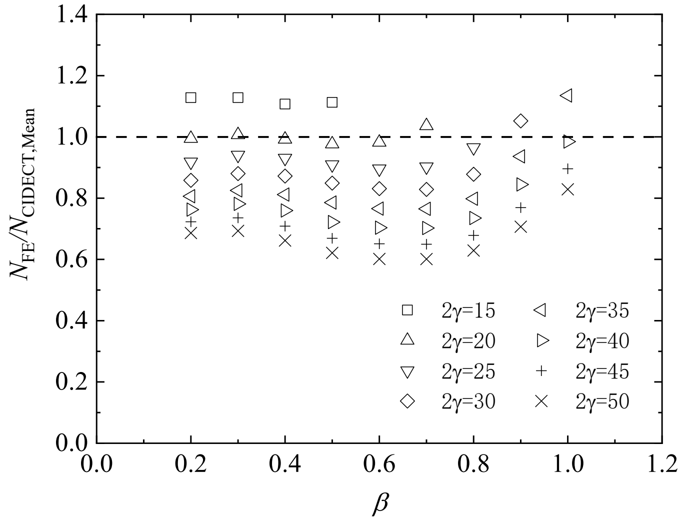

(b) S700

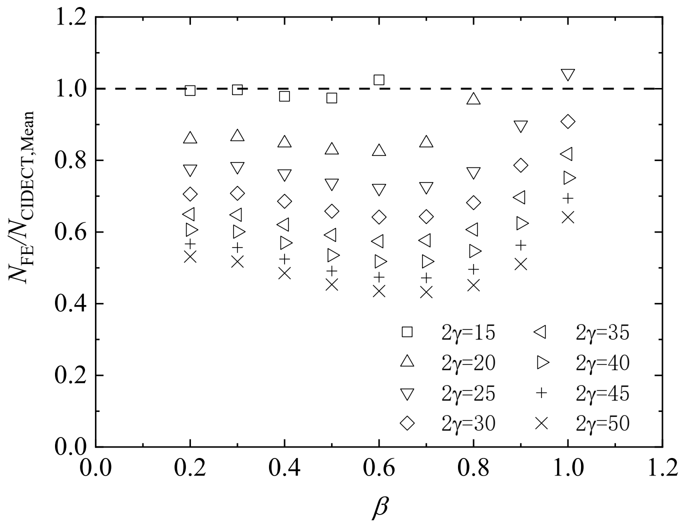

(c) S900

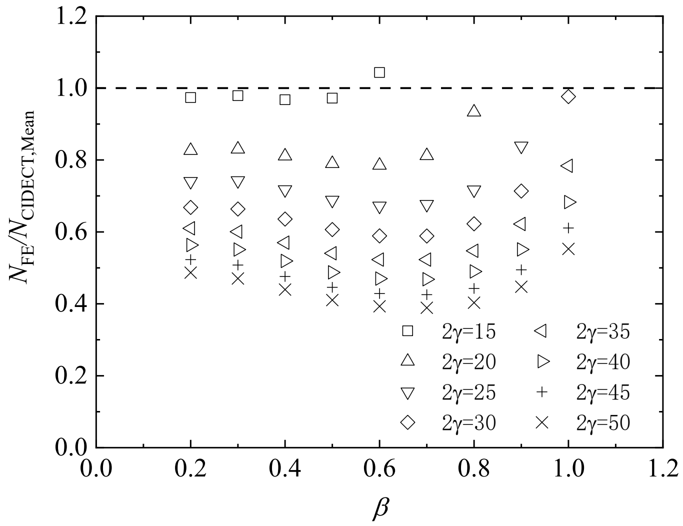

(d) S1100

Fig. 10. Comparison of CIDECT mean strengths with FE strengths for HSS CHS T-joints.

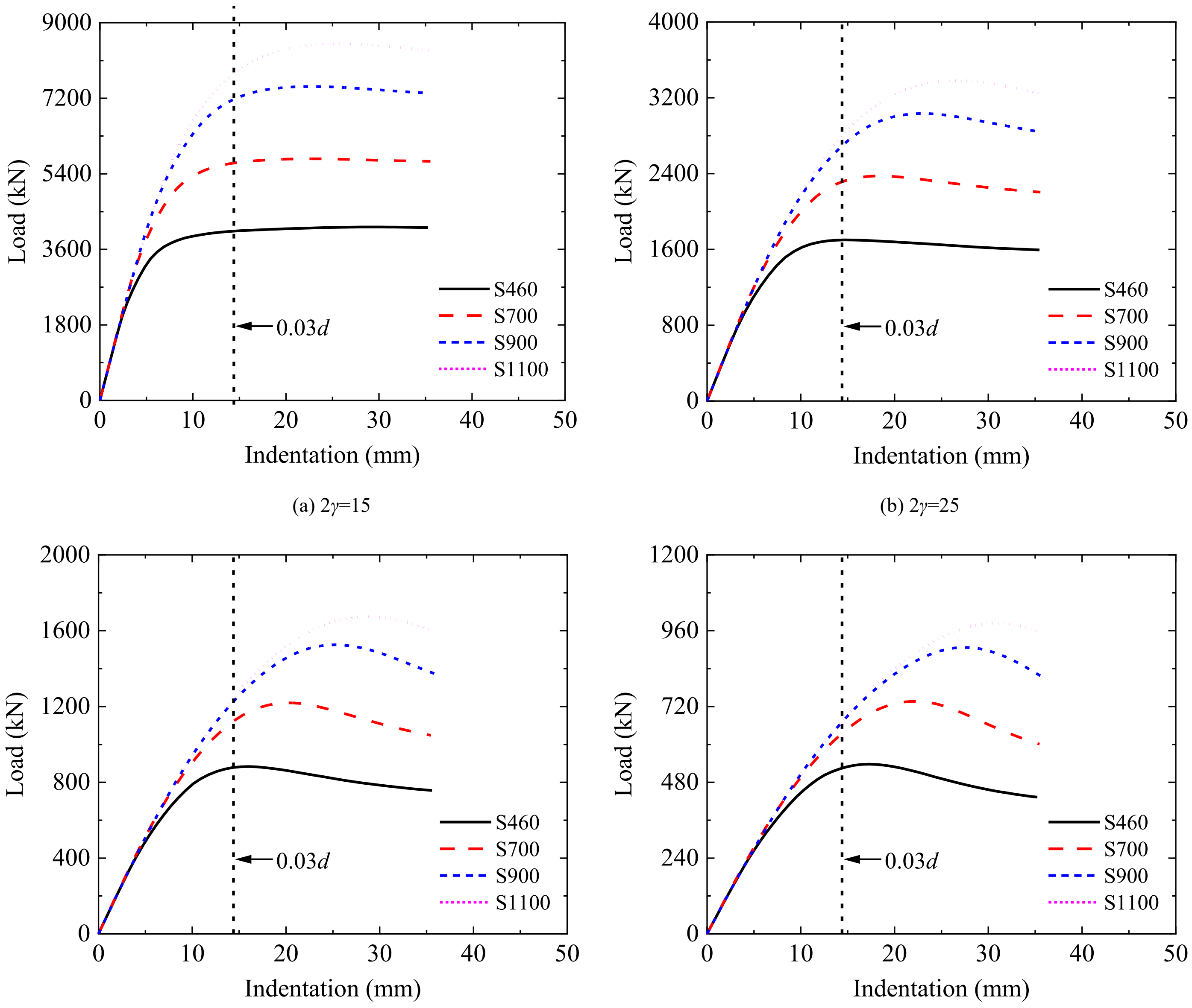

(a) 2γ=15 (b) 2γ=25

(c) 2γ=35 (d) 2γ=45

Fig. 11. Typical load-indentation curves of HSS CHS T-joints with β=0.4.

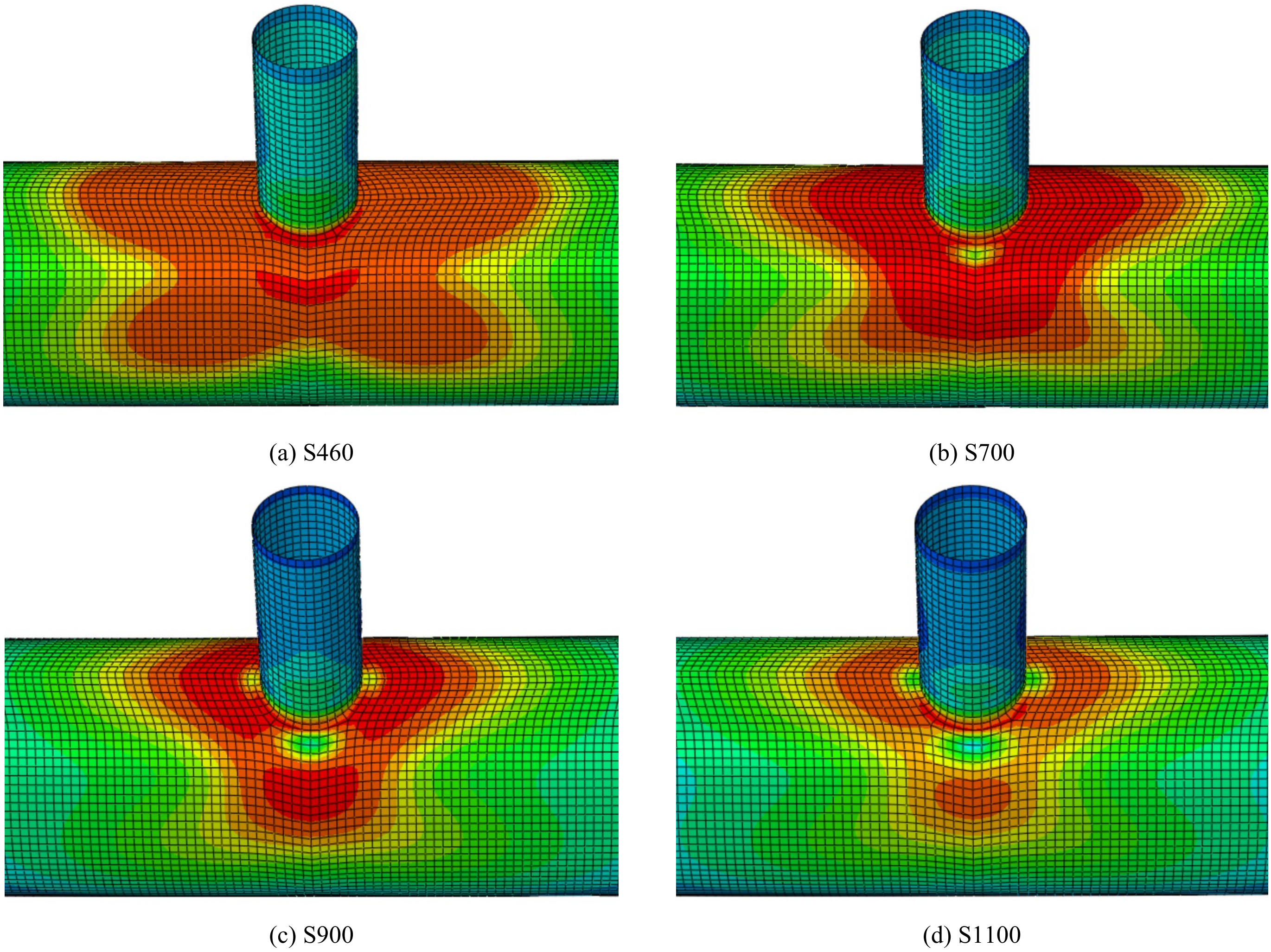

Fig. 12. Typical yielding patterns of HSS CHS T-joints with β=0.4 and 2γ=25 at the joint strengths.

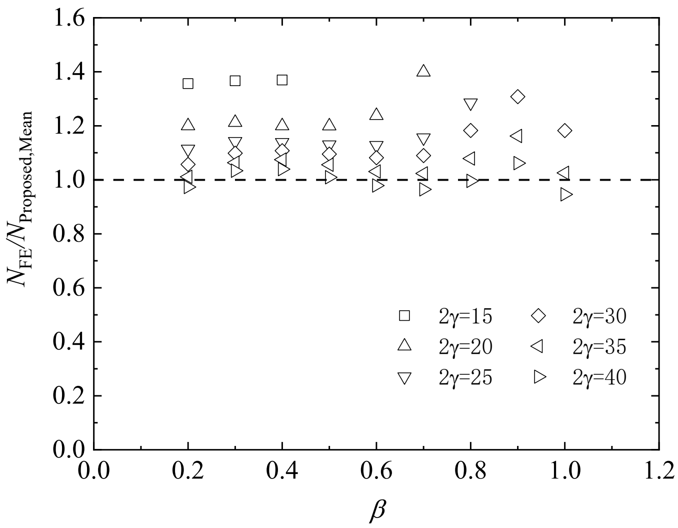

(a) S460

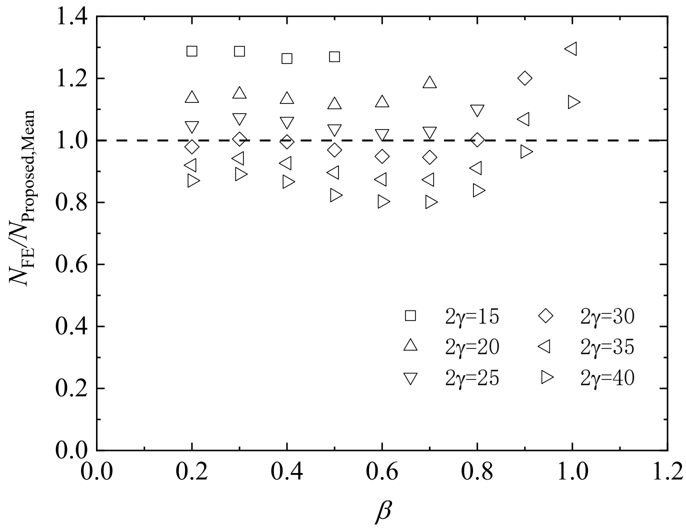

(b) S700

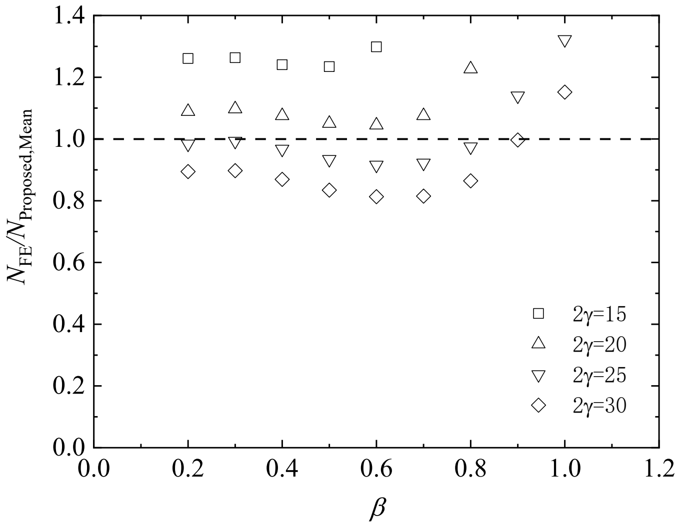

(c) S900

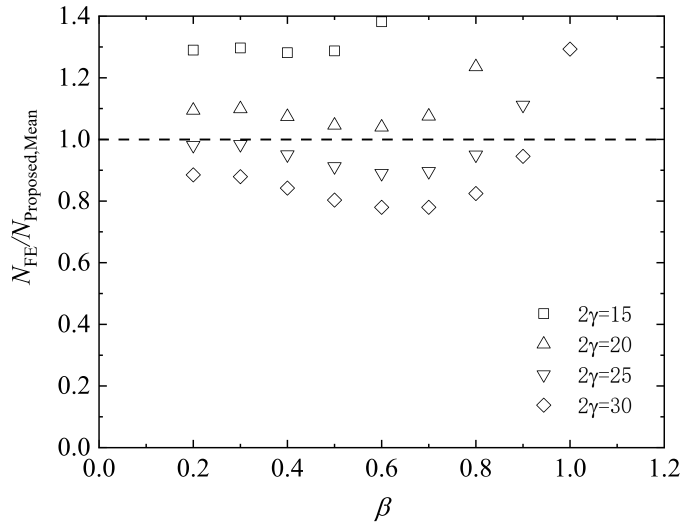

(d) S1100

Fig. 13. Evaluation of the proposed mean strength equation against FE results for HSS CHS T-joints.